Designing of UiO-66 Based Super Protonic Conductor with Highest MOF Based Proton Conductivity

Subhabrata Mukhopadhyay, Joyashish Debgupta, Chandani Singh, Rudraditya Sarkar, Olivia Basu, Samar K. Das*

*School of Chemistry, University of Hyderabad, Hyderabad – 500046, India

E-mail: skdas@uohyd.ac.in; samar439@gmail.com

KEYWORDS. MOF, Post synthetic modification, Superproton conductors, Humidity assisted Proton Conduction, Effect of chain length.

ABSTRACT: MOF based proton conductors have received immense importance recently. The present study endeavors to design two post-synthetically modified UiO-66 based MOFs and study the effects of their structural differences on their proton conductivity. UiO-66-NH_2 is modified by reaction with sultones to prepare two homologous compounds *i.e.,* **PSM 1** and **PSM 2**, which have SO_3H groups in comparable extent (Zr:S ≈ 2: 1) in both. But the pendant alkyl chain holding the –SO_3H group is of different length. **PSM 2** has longer alkyl chain attachment than that of **PSM 1**. This difference in length of side arm results in huge difference in proton conducting behavior of the two compounds. **PSM 1** is observed to have highest MOF based proton conductivity (1.64×10^{-1} Scm^{-1}) at 80 °C, which is comparable to commercially available Nafion while **PSM 2** shows significantly lower conductivity. Again, the activation energy for proton conductivity is one of the lowest among all MOF based proton conductors in case of **PSM 1** while, **PSM 2** requires larger activation energy (almost three times).This profound effect of variation of chain length of side arm by 1 carbon atom in case of **PSM 1** and **PSM 2** was rather surprising and never documented before. This effect of length of side arm can be very useful to understand proton conduction mechanism of MOF based compounds and also to design better proton conductors. Besides, **PSM 1** showed proton conductivity as high as 1.64×10^{-1} Scm^{-1} at 80 °C temperature, which is the highest reported value till date among all MOF based systems. The lability of the –SO_3H proton of the post synthetically modified UiO-66 MOFs has theoretically been determined by molecular electrostatic potential (MEP) analysis and theoretical pK_a calculation of models of functional sites along with relevant NBO analyses.

INTRODUCTION

Transportation of protons plays a key role in photophosphorylation to harvest solar energy *via* ADP to ATP conversion.[1-3] Concentration gradient regulated proton transport through channels in cellular membrane is essential in energy transfer processes of organisms.[2] Apart from this fundamental function, efficient proton transport is also crucial for development of fuel cells, which can be one potential source of alternative energy in recent future. Different light and heavy vehicles are major reason behind high consumption of fossil fuels and environmental pollution too. Replacement of conventional engines by fuel cells is the best potential solution to this problem. Designing of novel fuel cell requires efficient proton conducting solid electrolyte.[4,5] All these factors make the study of proton conducting materials and proton transport very important for fundamental as well as applied science.[1-6]

Plenty of reports on new and efficient proton conductors in last five years, clearly establishes the increasing importance of this field in recent times.[7-27] Meanwhile, a lot of effort has also been devoted within last decade to contribute to the understanding of proton conduction mechanism.[28-36] The most common method of proton conduction is solvent assisted proton transfer.[1,2] Similar mechanism has been found to operate in most of the Brønsted acids, common protonic solvents and functionalized polymers.[29,31,33,34] Apparently, protonic solvents and Brønsted acids have the simplest structures among all; but, on the contrary, they are found to follow complicated conductive mechanism.[3,29-31] Since the last few decades, organic polymeric compounds (*e.g.,*Nafion) are well established as the supreme proton conductors. They possess conductivity of the order of 10^{-1} Scm^{-1} under humidification.[6] The problem associated with their practical usage is, their high manufacturing cost and lack of scope to tune their conductivities. On the other hand, detailed structural information is available for the mixed metal oxides and inorganic cluster containing compounds as they are crystalline in nature. But they are less popular as proton conductors due to low efficiency at ambient conditions.[30-32]

In this scenario, metal organic frameworks (MOFs) stand as a connecting bridge between inorganic cluster containing compounds and organic polymers in terms of detailed structural information from crystal structure and

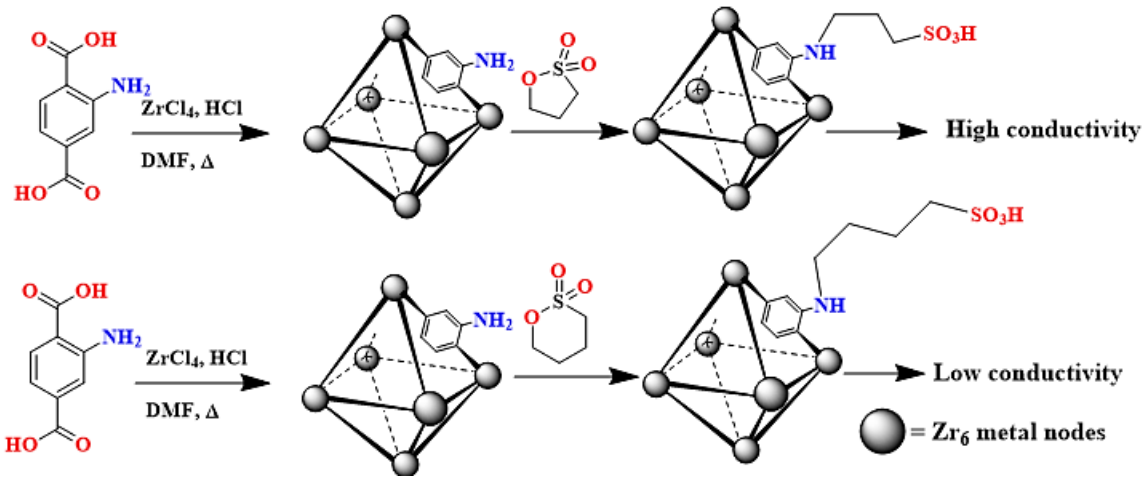

Scheme 1. Synthesis of UiO-66-NH_2 and its post synthetic modification to **PSM 1** (top) and **PSM 2** (bottom)

efficiency of proton conduction.[37-53] These MOFs, being polymeric hybrid of organic linker molecule and metal ions, cultivate some of the useful properties of both.[3,6] They have high thermal stability, tunable dimensionality of channels, provision to modify the organic linkers to impart selective functionality, scope of loading charge carrier ion and also the provision to incorporate Brønsted acidity inside the MOF cavity.[11,13,27,53] UiO-66, a renowned subclass of MOFs, has emerged as a high potential material to prepare highly efficient proton conductors.[41-45] UiO-66 consists of cationic $\{Zr_6O_4(OH)_4\}$ nodes connected to each other by BDC (benzenedicarboxylic acid)-based ligands.[61-62] Different derivatives of UiO-66 type MOFs have been reported in literature, where the BDC ligand was functionalized by different groups *e.g.*, amines, carboxylic acids, sulphonic acids, anhydrides, halogens *etc.*[54-56] Suitable water adsorptivity, existence of empty hydrophilic channels and scope to modify the pores by post synthetic modifications are some of the major reasons behind the notable domination by UiO-66 derivatives in the field of MOF based proton conductions.[42,44,57-58] Plenty of reports on UiO-66 based proton conductors are available in literature with conductivity values varying in a wide range of 10^{-5} Scm^{-1} to 10^{-2} Scm^{-1}.[41-45] Researchers have tried to explore different structural properties and synthetic modifications to design more efficient UiO-66 based functional materials.[57,58] For quite a long time, isomorphous ligand replacements, organic linker modifications, enhancement of crystal defects and loading of different guest molecules (e.g., histamine, triazole, *etc.*) have served as well-known paths to prepare MOF based proton conductors.[37,38,40-42,59]

A very recent report by Shimizu and co-workers has demonstrated that the bulk conductivities of two MOF materials, PCMOF2$^{1/2}$(Pz) and PCMOF2$^{1/2}$(Tz) (Pz = 1H-pyrazole and Tz = 1H-1,2,4-triazole), are over 10^{-1} S cm^{-1} at 85 °C and 90% relative humidity.[60] Earlier, Yang *et al.* showed a sulphonic acid rich flexible MOF, BUT-8(Cr)A to have conductivity of 1.27 × 10^{-1} Scm^{-1} (at 80 °C under 100% relative humidity), the highest reported proton conductivity, exhibited by any MOF material except **PSM 1** reported in this work.[61] Few years ago, Hong and coworkers showed UiO-66$(SO_3H)_2$ to possess conductivity of 8.4×10^{-2} Scm^{-1}.[44] High loading of pendant sulphonic acid groups played crucial role behind this observed proton conductivity. Li and coworkers developed another UiO-66 based proton conductor by its functionalization.[43] It was established from the same work that Brønsted acidic groups, dangling inside from the walls of the channels, helps the protonation and deprotonation steps required for proton flow through the preformed aqua-chain under high humidity. It was also shown that, the proton conduction was directly related with the water sorptivity of UiO-66 derivative. In a complete different approach, Kitagawa and co-workers showed that, controlling the mobility of proton can also be fundamentally important apart from enhancing Brønsted acid concentration to control the proton conductivity of a MOF.[42]

Focusing on the contemporary works on UiO-66 based proton conductors, our attention was drawn to the fact that, even though, enormous significance of the pendant Brønsted acid has been established,[59] not much efforts have been given to recognize the effect of chain length of the arm (attached to the rigid framework in one end and holding the acid group in the other end) on proton conductivity. In this present work, we have put an effort to study it and attempted to combine the missing dots in order to get the complete picture.

We prepared (Scheme 1) two post synthetically modified UiO-66 MOFs (hereafter referred as **PSM 1** and **PSM 2**) with variation in chain length of side arm holding the Brønsted acid group. Choice of post synthetic modification (PSM) over preformed BDC derivative was crucial to nullify incorporation of any unwanted structural differences (*i.e.*, crystal defects *etc.*). The choice was also influenced by recent works of Garibay,

Cohen and co-workers, who reported various crucial post synthetic functionalizations on UiO-66 that, are difficult otherwise.[56]

The two sister compounds, reported here *i.e.,* **PSM 1** and **PSM 2**, were synthesized by adapting a highly reproducible two step synthetic method, where both the steps were well established in previous reports but never combined together to prepare any MOF based proton conductors. Thus prepared, **PSM 1** is found to be a MOF based super proton conductor, having the highest conductivity among all MOFs. We have also demonstrated the profound effect of chain length of side arm on efficiency of proton conductivity of the MOF.

MATERIALS AND METHODS

Synthesis of UiO-66-NH_2, **PSM 1**, **PSM 2** and **PSM 1**-Li

To obtain the post synthetically modified compounds, first UiO-66-NH_2 was prepared following the procedure, reported by Farha and coworkers.[62] In a typical synthesis, 5.4 mmol of $ZrCl_4$ was dissolved in 50 mL DMF in presence of 10 mL of conc. HCl by sonication. Then 6.75 mmol BDC-NH_2(BDC = benzene dicarboxylic acid) was added along with 100 mL of DMF. The reaction mixture was kept at 80 °C temperature for 24 hours in a sealed Teflon capped container of 250 mL. After slow cooling, the reaction mixture was filtered and washed. Subsequently, the crude UiO-66-NH_2 was stirred in dry ethanol for 72 hours to remove absorbed DMF molecules prior to post synthetic modifications and further characterizations. See section S2, Supporting Information for detailed synthetic procedure.

Fully activated and characterized UiO-66-NH_2 micro crystals were then separately treated with 1,3-propane sultone and 1,4-butane sultone to obtain **PSM 1** and **PSM 2** respectively (Scheme 1). This scheme of post synthetic modification was adapted from the work of Yaghi and coworkers.[63] Similar post synthetic modifications are well established in recent times.[64-66] In a typical PSM procedure, UiO-66-NH_2 and sultone were taken in DCM in equimolar ratio at room temperature (30 °C). After 24 hours, the post synthetically modified compounds were repeatedly washed with DCM, water and ethanol to get rid of any unreacted and trapped sultone/ hydrolyzed sulfonic acid from the pores. For detailed synthetic procedure, see section S2, Supporting Information.

PSM 1-Li was prepared by ion exchange between the labile protons of **PSM 1** and Li^+ ion. **PSM 1** was stirred in 0.5 M aqueous solution of LiCl for 24 hours. The modified compound *i.e.,* **PSM 1-Li** was washed thoroughly with water after the completion of ion exchange.

Physical Characterization

All the four compounds, UiO-66-NH_2, **PSM 1**, **PSM 2** and **PSM 1-Li** were thoroughly characterized by powdered XRD analysis, UV-Vis diffused reflectance spectroscopy, X-ray photoelectron spectroscopy, FT-IR spectroscopy, AES-ICP, FESEM-EDX and digestive NMR analysis. Gas and water sorption measurements, TG analysis and impedance spectroscopic measurements were done when they were required.

Proton Conductivity Measurements

Proton conductivity of UiO-66-NH_2, **PSM 1**, **PSM 2** and **PSM 1-Li** were measured by alternating current (AC) impedance spectroscopy using 2-electrode configuration (parallel plate mode). Samples were pelletized from their powdered microcrystals and sandwiched between two carbon papers (to lower the contact resistance between the electrodes and the sample and also to minimize probable artefacts originating from the sample surface inhomogeneity) before putting inside a home-made cell with 2 electrode set up. Powdered sample was kept under a pressure of 5 ton/ cm^2 for 3 minutes to prepare each sample pellet. Impedance spectra were recorded in the temperature range from 10 °C to 80 °C and relative humidity (RH) range of 30% to 95%. A programmable incubator was employed to keep the sample pellet at desired temperature and humidity for proton conductivity measurement. For higher temperature measurements i.e., ≥50 °C a home-made set up was used to stabilize the temperature and humidity instead of the incubator. For details of electrode set up, pellet preparation, impedance measurement parameters, incubation process *etc.*, see section S13 in Supporting Information. Impedance spectra were recorded for **PSM 1** and **PSM 2** during both the heating and cooling cycles. Reusability of the proton conductors was examined by recording four consecutive heating and cooling cycles for both **PSM 1** and **PSM 2**. Long term stability of the conductors was checked by proton conductivity measurements in constant time interval, while the sample was kept in the humidified elevated temperature throughout the whole period. Conductivity calculations were done from the Nyquist plots of impedance spectra by fitting with the most suitable equivalent circuit.

RESULTS AND DISCUSSION

As shown in Figure 1, the PXRD patterns of **PSM 1** and **PSM 2** were found to match well with the simulated one of UiO-66 MOF. After post synthetic modifications, they possess no notable change from the parent UiO-66-NH_2 pattern, signifying the integrity of the UiO-66 framework to be maintained. It shows that, the employed post synthetic modification does not disturb the crystal structure of UiO-66-NH_2.

All the compounds were found to retain their crystalline nature even after 1 year of keeping in open air (see Section S6, Supporting Information).

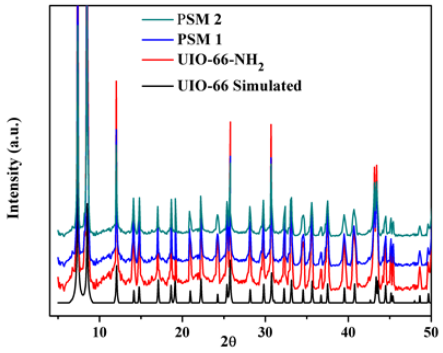

Figure 1. Powdered XRD patterns of UiO-66-NH_2, **PSM 1** and **PSM 2** compared with simulated pattern of UiO-66.

The crystallinity and structure of **PSM 1** and **PSM 2** were not disturbed significantly under high temperature or under high pressure (see Section, S6, Supporting Information). The compounds **PSM 1** and **PSM 2** were found to retain their structure even after 7 days of aqua-treatment at high temperature.

From XPS spectra of **PSM 1** and **PSM 2**, binding energy for $S2p_{3/2}$ peak was found at 168.3 eV and 168.0 eV, respectively. This is a clear proof of +IV oxidation state of sulfur in both; hence the presence of SO_3H group is confirmed (Figure 2). Furthermore, the N1s spectrum of **PSM 1** shows strong peak at 401.9 eV with a shoulder at 400.9 eV, similar to **PSM 2** but distinctly different from UiO-66-NH_2 primary amine peak. The XPS spectra are indicative of the presence of **(1)** secondary amine of the type '-CH-NH-CH_2-' (400.9 eV and 400.7 eV for **PSM 1** and **PSM 2** respectively) and **(2)** primary amine '-NH_2' (401.9 eV) in both. The huge shift in primary amine peak in **PSM 1** and **PSM 2**, compared to that of UiO-66-NH_2 can be a direct consequence of strong H-bonding with the adjacent –SO3H group of dangling side arm. Such XPS spectral shift due to H-bond formation is not uncommon for metal oxides, hydroxides and organic molecules but has not been documented before for UiO-66 MOF system.[67] Such extensive H-bonding can facilitate the aqua chain formation by fragmenting the long channel into smaller hydrophilic compartments.

The XPS spectral shift between secondary amine peak of **PSM 1** and **PSM 2** can be accounted qualitatively by the theoretical natural bond orbital (NBO) analysis on the

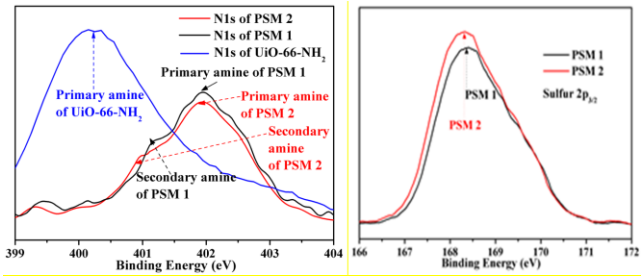

Figure 2. N1s (left), $S2p_{3/2}$(right) X-ray photoelectron spectra of **PSM1** and **PSM 2**.

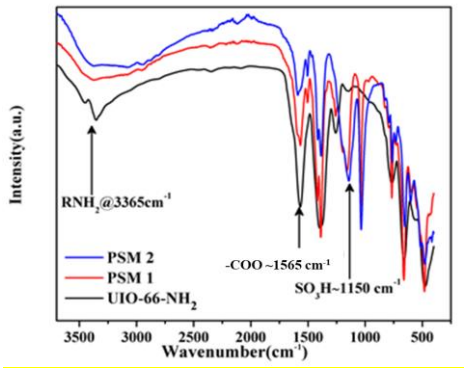

Figure 3. FT-IR spectra of UiO-66-NH_2, **PSM 1** and **PSM 2**.

model dangling parts of **PSM 1** and **PSM 2**. The core molecular orbital (which consists of 100% characteristic of N1s) of **PSM 1** is found to be more stable than that of **PSM 2** by ~0.0024 eV. It is noted that the calculated XPS spectral shift from NBO analysis qualitatively explains the observation obtained from the experiment as the calculations were performed on the model compounds in gas phase, while the experiment was carried out on the actual compounds in solid phase. Overall, the present theoretical prediction helps to understand the observed XPS spectral shift.

The FT-IR spectra (Figure 3) of UiO-66-NH_2, **PSM 1** and **PSM 2** are found to have notable similarities. The peak at 1565 cm^{-1}, because of the 'C=O' bond of carboxylate linkage, is present in all three spectra. In contrast, the peaks at ~3365 cm^{-1} arising from the primary '–NH_2' functional group of UiO-66-NH_2, is not visible in case of **PSM 1** and **PSM 2**. This is because of the post synthetic modification of half of the '-NH_2' groups of UiO-66-NH_2 during formation of **PSM 1** and **PSM 2**. As a result of addition of hydrophilic '-SO_3H' group *via* post synthetic modification, water content increases inside **PSM 1** and **PSM 2** under normal aerial conditions. Extensive H bonding interactions between '-OH' of '-SO_3H' groups mask all other peaks lying in this region. Due to '-SO_3H' group, two peaks near 1037 cm^{-1} and 1150 cm^{-1} can be found both in **PSM 1**and **PSM 2**. As expected, these peaks are not present in FT-IR spectrum of UiO-66-NH_2(Figure 3). From both the XPS and FT-IR data, we infer successful post synthetic modification of UiO-66-NH_2 to prepare **PSM 1** and **PSM 2** while keeping the basic UiO-66 intact.

We have performed digestive NMR and ESI-MS spectral analyses. For detailed procedure see section S12, Supporting Information. Both the ^{1}H NMR spectra and ESI-MS spectra of **PSM 1** and **PSM 2** show the presence of impurities generated due to uncontrolled fragmentation of the compound during digestion in HF. Even then, peaks due to the desired fragments *i.e.,* the aromatic ring and alkyl side arm, can be identified from the ^{1}H NMR spectra of **PSM 1** and **PSM2**. ESI-MS spectra of **PSM 1** and **PSM 2** show high intensity peaks at m/z value of 303.48 and 317.02 respectively. The peak positions match well with the mass of expected fragments in each case. Thus,

digestive NMR and ESI-MS data support the structural analysis, obtained from other physical characterization techniques. ICP-AES analysis was performed to have further structural insight about the Brønsted acid loading in **PSM 1** and **PSM 2**. It was found that, the extent of PSM was consistent with the atomic ratio of S:Zr ≈ 1:2 in both the compounds (from ICP-AES analysis) and weight percent of sulfur was found to be 5.02 % and 5.03% in **PSM 1** and **PSM 2**, respectively (see section S8, Supporting Information). The two factors, *i.e.,* (i) the employment of same UiO-66-NH_2 microcrystals for PSM and (ii) similar Brønsted acid loading in both **PSM 1** and **PSM 2**, are helpful to evaluate proton conductivity only on the basis of side arm length and ignore any variance in contribution from other factors. Furthermore, it could also be confirmed from ICP-AES analysis that, only half of the '-NH_2' groups of UiO-66-NH_2 are modified in both cases (**PSM 1** and **PSM 2**). These results also enlighten the fact of low Brønsted acid loading (almost one fourth) when compared with the similar system UiO-66$(SO_3)_2$, reported by Phang *et al.*[44]

As the PSM is supposed to increase steric bulk inside the cavities of **PSM 1** and **PSM 2** from that of UiO-66-NH_2 parent MOF, large variation in the permanent porosity could be expected. N_2 gas sorption measurement at 77 K was used as the tool to determine permanent porosity of all the MOFs (Figure 4(a)). Prior to gas adsorption studies, UiO-66-NH_2, **PSM 1** and **PSM 2** were degassed for 10 hours under vacuum at 120 °C (for details see section S9, Supporting Information). All three gas adsorption isotherms follow Type-I behavior, confirming presence of micropores. Inter-grain sorption (typical phenomenon of microporous materials) results in the rapid rise of isotherm around P/Po= 0.9-1 for all the three compounds (Figure 4(a)). Brunauer-Emmett-Teller (BET) surface analysis from N_2 sorption studies reveal that, **PSM 1** (surface area 328.5 m^2/g) is having slightly higher available surface area for N_2 sorption than that of **PSM 2** (surface area 294.3 m^2/g). But both of them are having surface area much lower than that of UiO-66-NH_2 (surface area 684.5 m^2/g). The significant decrease in BET surface area of ≈370 m^2/g in **PSM 1** and **PSM 2** from that of UiO-66-NH_2 is a direct consequence of less availability of free space due to impregnation of long side arms inside the pores of **PSM 1** and **PSM 2**. BET surface areas of **PSM 1** and **PSM 2** differs by 34.2 m^2/g, which can be attributed to the more bulkiness of the side arm of **PSM 2** as well as minutely higher loading in case of **PSM 2** (*vide supra*) than **PSM 1**.

As mentioned above, the BET surface area of UiO-66-NH_2 itself (684.5 m^2/g) was found to be lower than that shown in similar recent reports.[41-44] In order to have more insight into this surface area profile, the same UiO-66-NH_2 was characterized by N_2 sorption measurement after activating the compound at 180 °C for 6 hours. And in this case, BET surface area for the same UiO-66-NH_2 was recorded to be 1086 m^2/g. Thus, the lower surface area

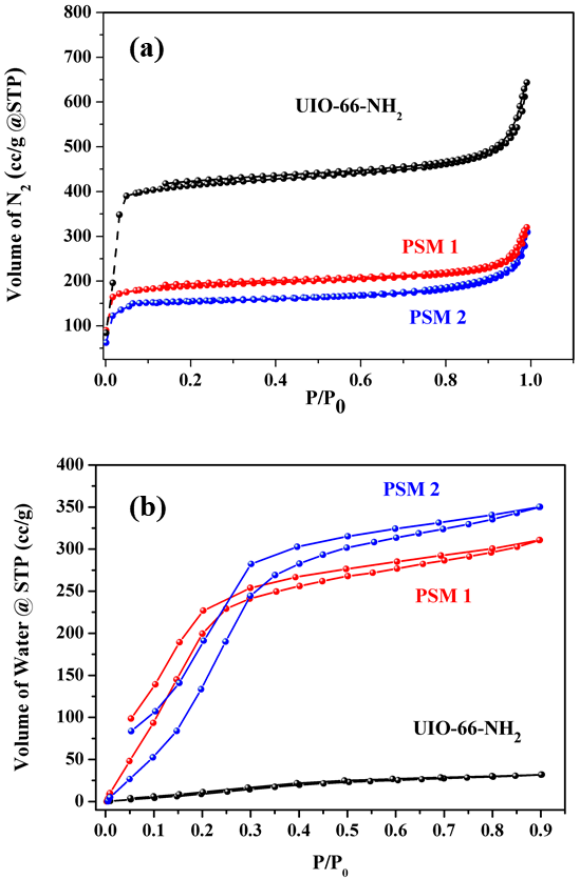

Figure 4. (a) N2 sorption isotherms and (b) water sorption isotherms of **PSM 1**, **PSM 2** and UiO-66-NH_2.

(684.5 m^2/g) obtained before was a result of activation of UiO-66-NH_2 in relatively lower temperature and not due to lack of crystalinity of the parent MOF, UiO-66-NH_2.

All the UiO-66 based MOFs have good water adsorptivity. And the post synthetically modified UiO-66-NH_2 derivatives show even superior water adsorptivity (Figure 4(b)) and notable aqua-stability (discussed earlier). Water adsorptivity is of immense importance in case of water assisted proton conduction, because adsorbed water molecules help the proton conductor to build continuous hydrogen-bonded network/chain along proton-propagating pathways. Under identical humidity (P/Po = 0.5), both the post synthetically modified compounds, **PSM 1** and **PSM 2** are found to show almost a 10-fold increase in the water uptake than that of UiO-66-NH_2 as shown in Figure 4(b). Slopes of water adsorption isotherms of **PSM 1** and **PSM 2** are found to be similar and almost 12 fold to that of pristine UiO-66-NH_2. High slope of water adsorption isotherms of **PSM 1** and **PSM 2**, even in moderate humidity, indicates their enhanced hydrophilic nature. Among **PSM 1** and **PSM 2**, **PSM 2** has slightly higher water sorption capacity than **PSM 1**, which might be a result of slight higher loading of $-SO_3H$ pendant groups in **PSM 2**. These results indicate that, PSM plays a vital role not only to incorporate Brønsted acidity but also to increase hydrophilicity. Thus, water

adsorption studies gave us a preliminary idea of the high potential of **PSM 1** and **PSM 2** to have enhanced water mediated proton conductivity in comparison to pristine UiO-66-NH_2.

Proton Conductivity Measurement and Related Analyses

Proton conductivity of all the compounds were measured by impedance spectroscopy using technique mentioned earlier (*vide supra*) (for detailed methodology, see Section S13, Supporting Information). Nyquist plots were constructed on the complex plane of impedance between Z' (real part of impedance) and Z" (imaginary part of impedance). A semicircle of high radius of curvature and another one with low radius of curvature could be resolved in the Nyquist plots of impedance spectra of both the compounds. Inter-grain resistance and

electrode-electrolyte contact resistance are responsible for the low frequency region impedance spectra while resistance of the material corresponding to proton conduction contributes for the high frequency region of impedance spectra. Li substituted **PSM 1** *i.e.,* **PSM 1-Li** was prepared to understand the origin of proton conductivity: whether it is a result of Brønsted acidic groups or due to participation of any other mobile charge carriers (electrons, metal ions *etc.*), see section S13, Supporting Information. **PSM 1-Li** was prepared by substituting all the labile Brønsted acidic protons of **PSM 1** by lithium. **PSM 1-Li** shows no significant conductivity (conductivity observed to be ~10^{-6} Scm^{-1}; Figure S26, Supporting Information). Such low conductivity of **PSM 1-Li** clearly proves that, once the labile protons are substituted in **PSM 1** by Li, the conductivity decreases significantly. Thus, contribution from electronic conductivity or any other charge carriers can be neglected in case of **PSM 1**. The same logic can be applicable in case of **PSM 2**.

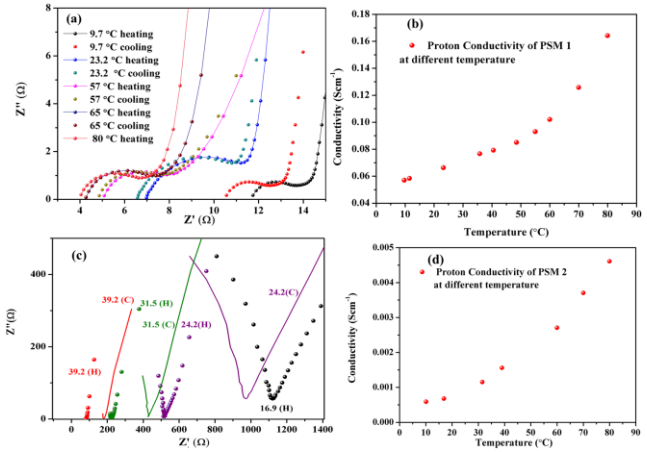

Figure 5. Nyquist plots of impedance spectra of **(a) PSM 1** and **(c) PSM 2**. Spectra were recorded at different temperatures during heating (spheres) and cooling (sphere with line) cycles. **(b)** and **(d)** shows the proton conductivity recorded during heating cycle of **PSM 1** and **PSM 2** respectively. Measurements were carried out at 95% relative humidity. Plots **(a)** and **(b)** were scaled arbitrarily to magnify the high frequency region of impedance spectra of **PSM 1** and **PSM 2**.

Temperature dependent proton conduction measurements (**Figure 5(a)&(b) and 5(c)&(d)**) have been carried out for both the compounds, **PSM 1** and **PSM 2**. The samples were kept at constant temperature and humidity (relative humidity) for 4 hours before recording each data. Both the compounds, **PSM 1** and **PSM 2** show steady increase in proton conductivity with increase in temperature. Measurements were carried out during both the heating and cooling cycles to check the reversibility of the performance. The Nyquist plots of heating and cooling cycle are similar to each other in terms of nature of curve, but, do not superpose (which it should, ideally). This deviation can be explained as a result of difference in water content inside the pores during heating and cooling cycles (see section S13, Supporting Information). Similar observations are quite common in MOF based proton conductors.[44] The observed proton conductivity was found to be retained for more than four consecutive heating and cooling cycles. Both **PSM 1** and **PSM 2** sample pellets were examined by PXRD and FT-IR analyses after proton conductivity measurements (see section S14, Supporting Information). PXRD and FT-IR spectra of the pelletized compounds showed no notable change even after 4 cycles. A lowering of ≈ 18m^2/g BET surface area is observed in case of **PSM 1** after 5 cycles of measurement. Such minor lowering of surface area indicates no major change in the microstructure of **PSM 1** in the end of proton conduction measurements. This lowering can be a result of the high pressure which is applied for pelletizing the compound before proton conductivity measurements. To check long term stability proton conductivity measurements were carried out for **PSM 1** at 80 °C for 48 hours. The data recorded at each 12 hours interval show very little fluctuation in proton conductivity. Please see Supporting Information Section S14 for detailed discussion.

Long term proton conductivity measurement of 48 hours along with the impedance measurement during consecutive 5 cycles of heating and cooling prove the stability and reusability of **PSM 1** and **PSM 2** as proton conductor. The similarities between the N_2-sorption isotherms, PXRD patterns and FT-IR spectra between the initially recorded ones and the ones recorded after each cycle of impedance measurement (Figure S27, Figure S28, Figure S29, and Figure S30, in Supporting Information) negate the chances of any major structural change. The results, thus obtained, establish the fact that both the compounds have the potential to function as stable proton conductors.

Experimentally obtained impedance spectral data were analyzed and fitted with the most relevant circuit (**(R1/Q1)+(R2/Q2)+Q3**) where **R1, R2**= resistance, **Q1, Q2, Q3** =Constant phase elements) (Figure6(a), inset) to calculate proton conductivity. All the experimentally obtained impedance spectral data could be fitted with the same circuit without notable error (in terms of χ^2 value). By fitting with equivalent circuit, it is found that, **PSM 1**

shows proton conductivity (σ) of 5.83×10^{-2} Scm^{-1} at 11.5 °C with 95% relative humidity (RH), while **PSM 2** has σ value of 5.9×10^{-4} Scm^{-1} at similar condition (10.1 °C, 95 %RH). The value of σ for **PSM 1** is, so far, the highest reported proton conductivity value for a MOF-like material at such a low temperature (10.1 °C), which is ~100 times of its sister compound *i.e.,* **PSM 2**.

At 80 °C, the proton conductivity was all the more pronounced for both the compounds than conductivities recorded at lower temperatures. The values of σ for **PSM 1** and **PSM 2** were 1.64×10^{-1} Scm^{-1} and 4.66×10^{-3} Scm^{-1} respectively. The value of σ for **PSM 1** at 80 °C is the highest among all MOF-based proton conductors (Table S12, Supporting Information). The proton conductivity of **PSM 1** is even comparable to that of commercially available organic polymeric conductor Nafion.[6]

Similar to most of the reported UiO-66 type proton conductors, **PSM 1** and **PSM 2** show water assisted proton conductivity[48-50] under humidified condition, as shown in Figure 6 (a) and Figure 6(b) respectively. Loading of Brønsted acidic '–SO_3H' functionalized side arms increases the amount of hydrophilic domains. Both **PSM 1** and **PSM 2** show excellent water adsorptivity (*vide supra*) in moderate to high humidity region ($P/P_o \approx 0.5$-0.7). Thus, proton conductivity of both the compounds was measured in wide range of relative humidity (from moderate to high), at 30°C (Figure 6). Conductivity was found to increase rapidly in moderate RH (from 30 % to 70 % RH). Slow but steady increment in conductivity was observed under high RH (80% to 95%) conditions (Figure S25). The enhancement of proton conductivity with increase in humidification, confirms a water assisted proton conduction in both **PSM 1** and **PSM 2**. Proton conduction can take place in a facile manner in these two compounds even in moderate humidity (~70% humidity). **PSM 1** has higher efficiency in terms of proton conductivity than **PSM 2** under all experimental conditions. Unlike proton conduction through grain boundary or *via* mobile guest molecules, these post synthetically modified compounds perform proton conduction with the help of covalently bound pendant '–SO_3H' groups *via* aqua channel formation (under humidification) inside the pores.

The water assisted proton conductivity of **PSM 1** can be compared to that of the UiO-66-$(SO_3H)_2$, reported by Hong and coworkers. Although, **PSM 1** has only one-fourth concentration of Brønsted acid groups than that, present in UiO-66$(SO_3H)_2$ but almost twice efficient in comparison to UiO-66$(SO_3H)_2$.[44] A comprehensive assessment of the two suggests that, the extent of availability of labile protons plays the most influential role in case of **PSM 1** and not the concentration of the Brønsted acid groups as, observed, in the case of UiO-66-$(SO_3H)_2$.[44]

It is quite interesting to note that, only a slight structural difference between **PSM 1** and **PSM 2** gives rise to the sharp variation in their observed proton conductivity. This is a unique observation in the area of MOF-based proton conductors, which again highlights the same fact of different extent of availability of the labile '–SO_3H' protons in **PSM 1** and **PSM 2**. Both these compounds have almost similar '-SO_3H' content but, show widely different proton conductivity, which can be a direct consequence of the difference in availability of labile protons and not the number of labile protons. Thus, in this present work, the effect of variation in chain-length of side arm (carrying the pendant Brønsted acid group) on proton conductivity of MOF based materials has been portrayed.

The variation in length of the dangling alkyl chains can result in change in several parameters *e.g.,* **(a)** difference in pK_a value of the Brønsted acid groups, **(b)** variation of hydrophobic steric bulk inside the pores among **PSM 1** and **PSM 2**, and **(c)** difference in H-bonding interactions between neighboring '-NH_2' and '-NH-$(CH_2)_3$-SO_3H' groups in case of **PSM 1** and '-NH_2' and '-NH-$(CH_2)_4$-SO_3H' groups in case of **PSM 2** *etc.* All these factors might contribute to

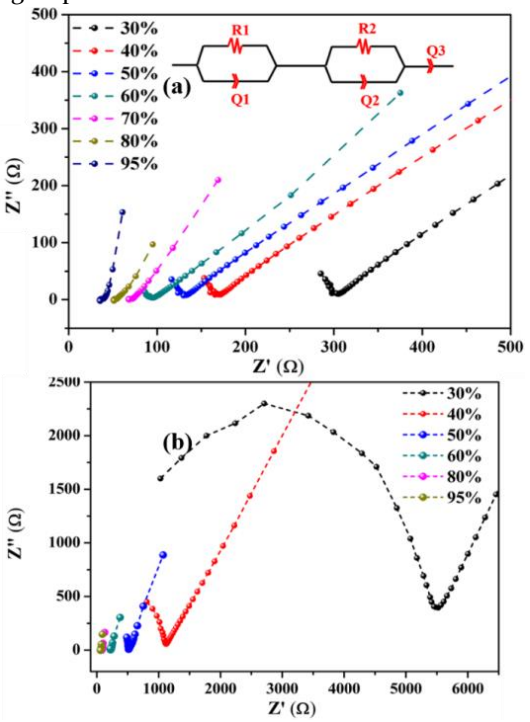

Figure 6. (a) Nyquist plot of impedance spectra of **PSM 1** under different humidification conditions at 30 °C. Inset: Equivalent circuit of impedance spectra of **PSM 1** and **PSM 2**. (b) Nyquist plot of impedance spectra of **PSM 2** under different humidification conditions at 30 °C.

the observed trend of proton-conductivity. Among all, one of the most crucial factors is the difference in pK_a value of **PSM 1**, **PSM 2** and UiO-66-NH_2. The theoretical pK_a values of the dangling '-SO_3H' group of **PSM 1**, **PSM 2** and '-NH_2' group of UiO-66-NH_2 are 3.47, 4.91 and 35.99, respectively (see section S17, Supporting Information). Lower the pK_a of a proton in a compound, higher is its lability, leading to higher proton conductivity. The pK_a values are in accord with the trend expected from observed proton conductivity. Along with that, the extensive compartmentalization due to H-bonding between the dangling -SO_3H and nearby -NH_2, enhances the proton conductivity of both **PSM 1** and **PSM 2**. On the other hand, the probability of any difference in the extent of H-bonding between **PSM 1** and **PSM 2** can be ignored because in both cases spectral shifts of N1s XPS spectra from the parent compound UiO-66-NH_2 are similar. Based on this XPS analysis (*vide supra*) it can be said that, the extent of H-bonding is similar in both **PSM 1** and **PSM 2**. This extensive H-bonding favours proton conduction in **PSM 1** as well as in **PSM 2** over UiO-66-NH_2, which cannot have such kind of H-bonding. Thus, negating any crucial role of factor **(c)** to decide the order/trend of proton conductivity among **PSM 1** and **PSM 2**, factor **(a)** (difference in pK_a) can be considered as the most important factor that explains the observed trend of proton conductivity among **PSM 1** and **PSM 2**. Again, we must mention that, contribution from other factors cannot be completely neglected.

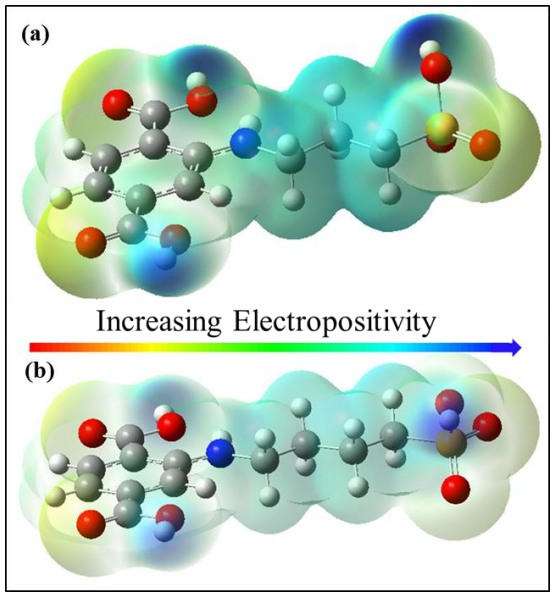

Figure 7. Molecular electrostatic potential (MEP) diagram of (a) BDC-NH-CH_2-CH_2-CH_2-SO_3H, and (b) BDC-NH-CH_2-CH_2-CH_2-CH_2-SO_3H. They are the two model compounds which represent the two post synthetically modified functional units of **PSM 1** and **PSM 2** respectively.

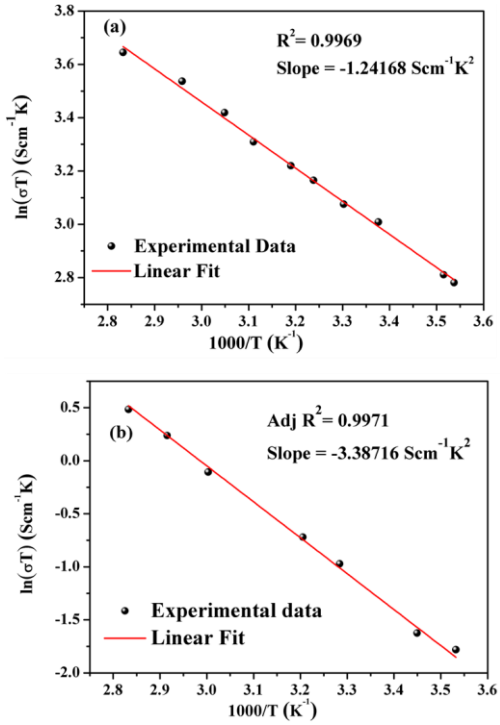

Figure 8. Arrhenius plots of temperature dependence of proton conduction of (a) **PSM 1** and (b) **PSM 2**.

Further, we confirm the lability of the '-SO_3H' proton of **PSM 1** and **PSM 2** by molecular electrostatic potential (MEP) of model compounds of functional units of **PSM 1** and **PSM 2**. NBO (natural bond order) analyses of the dangling part of **PSM 1** and **PSM 2** were also performed (see section S18, Supporting Information). The MEP plots (Figure 7) indicate higher electro-positivity on the '-SO_3H' proton of **PSM 1** (deep blue, Figure 7) as compared to the same of **PSM 2** (light blue, Figure 7). While, NBO analyses indicate higher charge transfer from the '–OH' oxygen to the '–OH' hydrogen of '-SO_3H' proton of **PSM 2** as compared to the same of **PSM 1**. This gives more stability to the dangling part of **PSM 2** by ~1.08 Kcal/mol. Thus, the '-SO_3H' proton of **PSM 1** becomes more labile than that of **PSM 2**. Thus, the theoretical studies on the model compounds of **PSM 1**, **PSM 2** and UiO-66-NH_2 partly explain the observed proton conductivity on the basis of charge distribution, pK_a and bond order calculations.

Activation energy (E_a) of proton conduction was calculated for **PSM 1** and **PSM 2**, based on the proton conductivity calculated for heating cycle (Figure 8(a) and Figure 8(b) respectively). For detailed calculation of activation energy, see section S15, Supporting Information. Activation energy (Ea) was found to be 0.107 eV/atom for **PSM 1** and 0.292 eV/atom for **PSM 2**. As the values suggest, both **PSM 1** and **PSM 2** follow water assisted Grotthuss mechanism for proton conduction. The activation energy for **PSM 1** is one of the lowest reported till date for any MOF based proton conductors (Table S12, Supporting Information). Low activation energy of

PSM 1 indicates the profound effect of easy availability of '-SO_3H' protons. Again, E_a values for **PSM 2** is almost 3 times higher than that for **PSM 1**. This is a consequence of only the structural difference *i.e.,* the difference in the chain length of the side arm. It is evident that **(1)** extensive H-bonding occurs for **PSM 1** as well as **PSM 2** and **(2)** the difference by one '–CH_2' unit in the side arm of **PSM 1** and **PSM 2** leads to difference in lability of proton of **PSM 1** and **PSM 2** (*vide supra*). As a result, proton conductivity is enhanced in both **PSM 1** and **PSM 2** than UiO-66-NH_2 but, **PSM 1** shows much higher conductivity and lower activation energy (mostly due to its lower pK_a) than **PSM 2**. Though, the exact reason is not yet known, but observing such huge difference in proton conductivity, just by increasing '–CH_2' fragment by one unit, is noteworthy.

CONCLUSION

We have prepared a super-proton conductor (**PSM 1**) with conductivity as high as 1.64×10^{-1} Scm^{-1}, which is the highest reported value till date among all other MOF based systems, operating below 100 °C. We also have shown that **PSM 2**, the homologous counterpart of **PSM 1**, has ~35 times lower proton conductivity than that of **PSM 1**. These observations clearly demonstrate the effects of length of side arm on the observed proton conductivity. We have shown by theoretical studies that, the difference in the chain length causes dramatic variation in pK_a values of the two compounds. The observed proton conductivity trend matches well with the order, expected from calculated pK_a. This observation is highly important to understand the role of the length of the side arm and design MOF based super proton conductors with higher efficiency performing at ambient temperature. This work has also highlighted the scope of employment of post synthetic modifications to UiO-66 and other MOF systems, so that, robust and more efficient MOF based proton conductors can be designed and developed.

ASSOCIATED CONTENT

Supporting Information: The Supporting Information is available free of charge on the ACS Publications website at DOI:

Instrumentation, synthesis of compounds (UiO-66-NH_2, **PSM 1**, **PSM 2** and **PSM 1-Li**), characterization (PXRD, TGA, FESEM-EDX analysis, Gas adsorption and water adsorption studies, FT-IR, AES-ICP, *etc.*), Proton conductivity measurements (impedance spectroscopy in different conditions), and supporting results(stability of pelletized sample, reusability of compounds as proton conductors *etc.*) are given in PDF format.

AUTHOR INFORMATION

Corresponding Author

* **skdas@uohyd.ac.in**

Present Address

School of Chemistry, University of Hyderabad, Hyderabad – 500046, India.

Author Contributions

The manuscript was written through contributions of all authors.

ACKNOWLEDGMENT

We thank **SERB, DST, Government of India** (**Project EMR/2017/002971**) for financial supports. S.M. thanks **DST-INSPIRE,** New Delhi, J.D. thanks **DSKPDF** Scheme, UGC, New Delhi for fellowships, C.S. thanks **UGC-BSR** and R.S. thanks **CSIR, New Delhi** for fellowship.

ABBREVIATIONS

BDC, benzenedicarboxlic acid; FT-IR, Fourier Transformed InfraRed; TGA, Thermal Gravimetric Analysis; AES-ICP, Inductively Coupled Plasmon Resonance Atomic Emission Spectroscopy; NMR, Neuclear Magnetic Resonance; XPS, X-Ray Photoelectron Spectroscopy; PXRD, Powdered X-Ray Diffraction; NBO, Natural Bond Order; MEP, Molecular electrostatic potential.

REFERENCES

(1) Kreuer, K.-D. Proton Conductivity: Materials and Applications. *Chem. Mater.* **1996**, *8*, 610–641.

(2) Barboiu, M.; Gilles, A. From Natural to Bioassisted and Biomimetic Artificial Water Channel Systems. *Acc. Chem. Res.* **2013**, *46*, 2814–2823.

(3) Ramaswamy, P.; Wong, N. E.; Shimizu, G. K. H. MOFs as Proton Conductors – Challenges and Opportunities. *Chem. Soc. Rev.* **2014**, *43*, 5913–5932.

(4) Scofield, M. E.; Liu, H.; Wong, S. S. A Concise Guide to Sustainable PEMFCs: Recent Advances in Improving Both Oxygen Reduction Catalysts and Proton Exchange Membranes. *Chem. Soc. Rev.* **2015**, *44*, 5836–5860.

(5) Fabbri, E.; Pergolesi, D.; Traversa, E. Materials Challenges toward Proton-Conducting Oxide Fuel Cells: A Critical Review. *Chem. Soc. Rev.* **2010**, *39*, 4355–4369.

(6) Laberty-Robert, C.; Vallé, K.; Pereira, F.; Sanchez, C. Design and Properties of Functional Hybrid Organic–inorganic Membranes for Fuel Cells. *Chem. Soc. Rev.* **2011**, *40*, 961-1005.

(7) Ranacher, C.; Resel, R.; Moni, P.; Cermenek, B.; Hacker, V.; Coclite, A. M. Layered Nanostructures in Proton Conductive Polymers Obtained by Initiated Chemical Vapor Deposition. *Macromolecules* **2015**, *48*, 6177–6185.

(8) Dawson, J. A.; Miller, J. A.; Tanaka, I. First-Principles Insight into the Hydration Ability and Proton Conduction of the Solid State Proton Conductor, Y and Sn Co-Doped $BaZrO_3$. *Chem. Mater.* **2015**, *27*, 901–908.

(9) Grancha, T.; Ferrando-Soria, J.; Cano, J.; Amorós, P.; Seoane, B.; Gascon, J.; Bazaga-García, M.; Losilla, E. R.; Cabeza, A.; Armentano, D.; Pardo, E. Insights into the

Dynamics of Grotthuss Mechanism in a Proton-Conducting Chiral BioMOF. *Chem. Mater.* **2016**, *28*, 4608–4615.
(10) Peng, Y.; Xu, G.; Hu, Z.; Cheng, Y.; Chi, C.; Yuan, D.; Cheng, H.; Zhao, D. Mechanoassisted Synthesis of Sulfonated Covalent Organic Frameworks with High Intrinsic Proton Conductivity. *ACS Appl. Mater. Interfaces* **2016**, *8*, 18505–18512.
(11) Inukai, M.; Horike, S.; Itakura, T.; Shinozaki, R.; Ogiwara, N.; Umeyama, D.; Nagarkar, S.; Nishiyama, Y.; Malon, M.; Hayashi, A.; Ohhara, T.; Kiyanagi, R.; Kitagawa, S. Encapsulating Mobile Proton Carriers into Structural Defects in Coordination Polymer Crystals: High Anhydrous Proton Conduction and Fuel Cell Application. *J. Am. Chem. Soc.* **2016**, *138*, 8505–8511.
(12) Yang, Y.; Sun, N.; Sun, P.; Zheng, L. Effect of the Bis-Imidazolium-Based Poly(Ionic Liquid) on the Microstructure and the Properties of AAEMs Based on Polyvinyl Alcohol. *RSC Adv.* **2016**, *6*, 25311–25318.
(13) Joarder, B.; Lin, J. Bin; Romero, Z.; Shimizu, G. K. H. Single Crystal Proton Conduction Study of a Metal Organic Framework of Modest Water Stability. *J. Am. Chem. Soc.* **2017**, *139*, 7176-7179.
(14) Wong, N. E.; Ramaswamy, P.; Lee, A. S.; Gelfand, B. S.; Bladek, K. J.; Taylor, J. M.; Spasyuk, D. M.; Shimizu, G. K. H. Tuning Intrinsic and Extrinsic Proton Conduction in Metal-Organic Frameworks by the Lanthanide Contraction. *J. Am. Chem. Soc.* **2017**, *139*, 14676–14683.
(15) Ma, H.; Liu, B.; Li, B.; Zhang, L.; Li, Y. G.; Tan, H. Q.; Zang, H. Y.; Zhu, G. Cationic Covalent Organic Frameworks: A Simple Platform of Anionic Exchange for Porosity Tuning and Proton Conduction. *J. Am. Chem. Soc.* **2016**, *138*, 5897–5903.
(16) Jiang, Z. J.; Jiang, Z.; Tian, X.; Luo, L.; Liu, M. Sulfonated Holey Graphene Oxide (SHGO) Filled Sulfonated Poly(Ether Ether Ketone) Membrane: The Role of Holes in the SHGO in Improving Its Performance as Proton Exchange Membrane for Direct Methanol Fuel Cells. *ACS Appl. Mater. Interfaces* **2017**, *9*, 20046–20056.
(17) He, G.; Xu, M.; Zhao, J.; Jiang, S.; Wang, S.; Li, Z.; He, X.; Huang, T.; Cao, M.; Wu, H.; Guiver, M. D.; Jiang, Z. Bioinspired Ultrastrong Solid Electrolytes with Fast Proton Conduction along 2D Channels. *Adv. Mater.* **2017**, *29*, 1605898.
(18) Klumpen, C.; Gödrich, S.; Papastavrou, G.; Senker, J. Water Mediated Proton Conduction in a Sulfonated Microporous Organic Polymer. *Chem. Commun.* **2017**, *53*, 7592–7595.
(19) Samanta, P.; Desai, A. V.; Anothumakkool, B.; Shirolkar, M. M.; Karmakar, A.; Kurungot, S.; Ghosh, S. K. Enhanced Proton Conduction by Post-Synthetic Covalent Modification in a Porous Covalent Framework. *J. Mater. Chem. A* **2017**, *5*, 13659–13664.
(20) Wu, H.; Yang, F.; Lv, X.-L.; Wang, B.; Zhang, Y.-Z.; Zhao, M.-J.; Li, J.-R. A Stable Porphyrinic Metal–organic Framework Pore-Functionalized by High-Density Carboxylic Groups for Proton Conduction. *J. Mater. Chem. A* **2017**, *5*, 14525–14529.
(21) Harada, A.; Shikinaka, K.; Ohshita, J.; Kaneko, Y. Preparation of a One-Dimensional Soluble Polysilsesquioxane Containing Phosphonic Acid Side-Chain Groups and Its Thermal and Proton-Conduction Properties. *Polym. (United Kingdom)* **2017**, *121*, 228–233.
(22) Mileo, P. G. M.; Kundu, T.; Semino, R.; Benoit, V.; Steunou, N.; Llewellyn, P. L.; Serre, C.; Maurin, G.; Devautour-Vinot, S. Highly Efficient Proton Conduction in a Three-Dimensional Titanium Hydrogen Phosphate. *Chem. Mater.* **2017**, *29*, 7263–7271.
(23) Qiu, X.; Ueda, M.; Hu, H.; Sui, Y.; Zhang, X.; Wang, L. Poly(2,5-Benzimidazole)-Grafted Graphene Oxide as an Effective Proton Conductor for Construction of Nanocomposite Proton Exchange Membrane. *ACS Appl. Mater. Interfaces* **2017**, *9*, 33049–33058.
(24) Sun, H.; Tang, B.; Wu, P. Two-Dimensional Zeolitic Imidazolate Framework/Carbon Nanotube Hybrid Networks Modified Proton Exchange Membranes for Improving Transport Properties. *ACS Appl. Mater. Interfaces* **2017**, *9*, 35075–35085.
(25) Dang, J.; Zhao, L.; Zhang, J.; Liu, J.; Wang, J. Imidazole Microcapsules toward Enhanced Phosphoric Acid Loading of Polymer Electrolyte Membrane for Anhydrous Proton Conduction. *J. Memb. Sci.* **2018**, *545*, 88–98.
(26) Wei, M.-J.; Fu, J.-Q.; Wang, Y.-D.; Zhang, Y.; Zang, H.-Y.; Shao, K.-Z.; Li, Y.-G.; Su, Z.-M. Highly Tuneable Proton-Conducting Coordination Polymers Derived from a Sulfonate-Based Ligand. *CrystEngComm* **2017**, *19*, 7050–7056.
(27) Ye, Y.; Guo, W.; Wang, L.; Li, Z.; Song, Z.; Chen, J.; Zhang, Z.; Xiang, S.; Chen, B. Straightforward Loading of Imidazole Molecules into Metal-Organic Framework for High Proton Conduction. *J. Am. Chem. Soc.* **2017**, *139*, 15604–15607.
(28) Takayanagi, M.; Tsuchiya, T.; Kawamura, K.; Minohara, M.; Horiba, K.; Kumigashira, H.; Higuchi, T. Thickness-Dependent Surface Proton Conduction in (111) Oriented Yttria-Stabilized Zirconia Thin Film. *Solid State Ionics* **2017**, *311*, 46–51.
(29) Melchior, J.-P.; Frick, B. On the Nanosecond Proton Dynamics in Phosphoric Acid–benzimidazole and Phosphoric Acid–water Mixtures. *Phys. Chem. Chem. Phys.* **2017**, *19*, 28540–28554.
(30) Uchida, S.; Hosono, R.; Eguchi, R.; Kawahara, R.; Osuga, R.; Kondo, J. N.; Hibino, M.; Mizuno, N. Proton Conduction in Alkali Metal Ion-Exchanged Porous Ionic Crystals. *Phys. Chem. Chem. Phys.* **2017**, *19*, 29077–29083.
(31) Foran, G. Y.; Brouwer, D. H.; Goward, G. R. Quantifying Site-Specific Proton Dynamics in Phosphate Solid Acids by ^{1}H Double Quantum NMR Spectroscopy. *J. Phys. Chem. C* **2017**, *121*, 25641–25850.
(32) Fluri, A.; Gilardi, E.; Karlsson, M.; Roddatis, V.; Bettinelli, M.; Castelli, I. E.; Lippert, T.; Pergolesi, D. Anisotropic Proton and Oxygen Ion Conductivity in Epitaxial $Ba_2In_2O_5$ Thin Films. *J. Phys. Chem. C* **2017**, *121*, 21797–21805.
(33) Chen, W.; Cui, F.; Liu, L.; Li, Y. Assembled Structures of Perfluorosulfonic Acid Ionomers Investigated by Anisotropic Modeling and Simulations. *J. Phys. Chem. B* **2017**, *121*, 9718–9724.
(34) Kuo, A.-T.; Tanaka, A.; Irisawa, J.; Shinoda, W.; Okazaki, S. Molecular Dynamics Study on the Mechanical Deformation of Hydrated Perfluorosulfonic Acid Polymer Membranes. *J. Phys. Chem. C* **2017**, *121*, 21374–21382.
(35) Jalili, J.; Coltelli, M. B.; Tricoli, V.; Orsini, G. Water-Free, Proton-Conducting Hybrid Materials for Elevated-Temperature Electrochemical Systems. *J. Phys. Chem. C* **2017**, *121*, 17129–17136.
(36) Economou, N. J.; Barnes, A. M.; Wheat, A. J.; Schaberg, M. S.; Hamrock, S. J.; Buratto, S. K. Investigation of Humidity Dependent Surface Morphology and Proton Conduction in Multi-Acid Side Chain Membranes by Conductive Probe

Atomic Force Microscopy. *J. Phys. Chem. B* **2015**, *119*, 14280–14287.
(37) Kim, S.; Dawson, K. W.; Gelfand, B. S.; Taylor, J. M.; Shimizu, G. K. H. Enhancing Proton Conduction in a Metal-Organic Framework by Isomorphous Ligand Replacement. *J. Am. Chem. Soc.* **2013**, *135*, 963–966.
(38) Pardo, E.; Train, C.; Gontard, G.; Boubekeur, K.; Fabelo, O.; Liu, H.; Dkhil, B.; Lloret, F.; Nakagawa, K.; Tokoro, H.; Ohkoshi, Shin, I.; Verdaguer, M.; High Proton Conduction in a Chiral Ferromagnetic Metal-Organic Quartz-like Framework. *J. Am. Chem. Soc.* **2011**, *133*, 15328–15331.
(39) Okawa, H.; Shigematsu, A.; Sadakiyo, M.; Miyagawa, T.; Yoneda, K.; Ohba, M.; Kitagawa, H. Oxalate-Bridged Bimetallic Complexes $\{NH(Prol)_3\}[MCr(Ox)_3]$ ($M=Mn^{II}$, Fe^{II}, Co^{II}; $NH(Prol)_3^+$ = Tri(3-Hydroxypropyl)Ammonium) Exhibiting Coexistent Ferromagnetism and Proton Conduction. *J. Am. Chem. Soc.* **2009**, *131*, 13516–13522.
(40) Umeyama, D.; Horike, S.; Inukai, M.; Hijikata, Y.; Kitagawa, S. Confinement of Mobile Histamine in Coordination Nanochannels for Fast Proton Transfer. *Angew. Chemie - Int. Ed.* **2011**, *50*, 11706–11709.
(41) Taylor, J. M.; Dekura, S.; Ikeda, R.; Kitagawa, H. Defect Control to Enhance Proton Conductivity in a Metal-Organic Framework. *Chem. Mater.* **2015**, *27*, 2286–2289.
(42) Taylor, J. M.; Komatsu, T.; Dekura, S.; Otsubo, K.; Takata, M.; Kitagawa, H. The Role of a Three Dimensionally Ordered Defect Sublattice on the Acidity of a Sulfonated Metal-Organic Framework. *J. Am. Chem. Soc.* **2015**, *137*, 11498–11506.
(43) Yang, F.; Huang, H.; Wang, X.; Li, F.; Gong, Y.; Zhong, C.; Li, J. R. Proton Conductivities in Functionalized UiO-66: Tuned Properties, Thermogravimetry Mass, and Molecular Simulation Analyses. *Cryst. Growth Des.* **2015**, *15*, 5827–5833.
(44) Phang, W. J.; Jo, H.; Lee, W. R.; Song, J. H.; Yoo, K.; Kim, B.; Hong, C. S. Superprotonic Conductivity of a UiO-66 Framework Functionalized with Sulfonic Acid Groups by Facile Postsynthetic Oxidation.*Angew. Chemie - Int. Ed.* **2015**, *54*, 5142-5146.
(45) Ragon, F.; Campo, B.; Yang, Q.; Martineau, C.; Wiersum, A. D.; Lago, A.; Guillerm, V.; Hemsley, C.; Eubank, J. F.; Vishnuvarthan, M.; Taulelle, F.; Horcajada, P.; Vimont, A.; Llewellyn, P. L.; Daturi, M.; Devautour-Vinot, S.; Maurin, G.; Serre, C.; Devic, T.; Clet, G.; Acid-Functionalized UiO-66(Zr) MOFs and Their Evolution after Intra-Framework Cross-Linking: Structural Features and Sorption Properties. *J. Mater. Chem. A* **2015**, *3*, 3294–3309.
(46) Shigematsu, A.; Yamada, T.; Kitagawa, H. Wide Control of Proton Conductivity in Porous Coordination Polymers. *J. Am. Chem. Soc.* **2011**, *133*, 2034–2036.
(47) Ramaswamy, P.; Wong, N. E.; Gelfand, B. S.; Shimizu, G. K. H. A Water Stable Magnesium MOF That Conducts Protons over 10^{-2} S Cm^{-1}. *J. Am. Chem. Soc.* **2015**, *137*, 7640–7643.
(48) Sahoo, S. C.; Kundu, T.; Banerjee, R. Helical Water Chain Mediated Proton Conductivity in Homochiral Metal-Organic Frameworks with Unprecedented Zeolitic Unh - Topology. *J. Am. Chem. Soc.* **2011**, *133*, 17950–17958.
(49) Sadakiyo, M.; Yamada, T.; Honda, K.; Matsui, H.; Kitagawa, H. Control of Crystalline Proton-Conducting Pathways by Water-Induced Transformations of Hydrogen- Bonding Networks in a Metal – Organic Framework Control of Crystalline Proton-Conducting Pathways by Water- Induced Transformations of Hydrogen-Bonding Network. *J. Am. Chem. Soc.* **2014**, *136*, 7701–7707.
(50) Morikawa, S.; Yamada, T.; Kitagawa, H. Crystal Structure and Proton Conductivity of a One-Dimensional Coordination Polymer, $\{Mn(DHBQ)(H_2O)_2\}$. *Chem. Lett.* **2009**, *38*, 654–655.
(51) Ramaswamy, P.; Matsuda, R.; Kosaka, W.; Akiyama, G.; Jeon, H. J.; Kitagawa, S. Highly Proton Conductive Nanoporous Coordination Polymers with Sulfonic Acid Groups on the Pore Surface. *Chem. Commun.* **2014**, *50*, 1144–1146.
(52) Yoon, M.; Suh, K.; Natarajan, S.; Kim, K. Proton Conduction in Metal-Organic Frameworks and Related Modularly Built Porous Solids. *Angew. Chemie - Int. Ed.* **2013**, *52*, 2688–2700.
(53) Bureekaew, S.; Horike, S.; Higuchi, M.; Mizuno, M.; Kawamura, T.; Tanaka, D.; Yanai, N.; Kitagawa, S. One-Dimensional Imidazole Aggregate in Aluminium Porous Coordination Polymers with High Proton Conductivity. *Nat. Mater.* **2009**, *8*, 831–836.
(54) Cavka, J. H.; Jakobsen, S.; Olsbye, U.; Guillou, N.; Lamberti, C.; Bordiga, S.; Lillerud K. P. A New Zirconium Inorganic Building Brick Forming Metal Organic Frameworks with Exceptional Stability. *J. Am. Chem Soc.* **2008**, *130*, 13850-13851.
(55) Yang, Q.; Wiersum, A. D.; Jobic, H.; Guillerm, V.; Serre, C.; Llewellyn, P. L.; Maurin, G. Understanding the Thermodynamic and Kinetic Behavior of the CO_2/CH_4 Gas Mixture within the Porous Zirconium Terephthalate UiO-66(Zr): A Joint Experimental and Modeling Approach. *J. Phys. Chem. C* **2011**, *115*, 13768–13774.
(56) Garibay, S. J.; Cohen, S. M. Isoreticular Synthesis and Modification of Frameworks with the UiO-66 Topology. *Chem. Commun.* **2010**, *46*, 7700–7702.
(57) Luan, Y.; Qi, Y.; Gao, H.; Andriamitantsoa, R. S.; Zheng, N.; Wang, G. A General Post-Synthetic Modification Approach of Amino-Tagged Metal-Organic Frameworks to Access Efficient Catalysts for the Knoevenagel Condensation Reaction. *J. Mater. Chem. A* **2015**, *3*, 17320–17331.
(58) Kandiah, M.; Usseglio, S.; Svelle, S.; Olsbye, U.; Lillerud, K. P.; Tilset, M. Post-Synthetic Modification of the Metal-Organic Framework Compound UiO-66. *J. Mater. Chem.* **2010**, *20*, 9848–9851.
(59) Jiang, J.; Yaghi, O. M. Brønsted Acidity in Metal-Organic Frameworks. *Chem. Rev.* **2015**, *115*, 6966–6997.
(60) Kim, S.; Joarder, B.; Hurd, J. A.; Zhang, J.; Dawson, K. W.; Gelfand, B. S.; Wong, N. E.; Shimizu, G. K. H. Achieving Superprotonic Conduction in Metal-Organic Frameworks through Iterative Design Advances. *J. Am. Chem. Soc.* **2018**, *140*, 1077–1082.
(61) Yang, F.; Xu, G.; Dou, Y.; Wang, B.; Zhang, H.; Wu, H.; Zhou, W.; Li, J. R.; Chen, B. A Flexible Metal-Organic Framework with a High Density of Sulfonic Acid Sites for Proton Conduction. *Nat. Energy* **2017**, *2*, 877–883.
(62) Katz, M. J.; Brown, Z. J.; Colón, Y. J.; Siu, P. W.; Scheidt, K. A.; Snurr, R. Q.; Hupp, J. T.; Farha, O. K. A Facile Synthesis of UiO-66, UiO-67 and Their Derivatives. *Chem. Commun.* **2013**, *49*, 9449–9451.
(63) Britt, D.; Lee, C.; Uribe-Romo, F. J.; Furukawa, H.; Yaghi, O. M. Ring-Opening Reactions within Porous Metal-Organic Frameworks. *Inorg. Chem.* **2010**, *49*, 6387–6389.
(64) Goesten, M. G.; Juan-Alcañiz, J.; Ramos-Fernandez, E. V.; Sai Sankar Gupta, K. B.; Stavitski, E.; Van Bekkum, H.; Gascon, J.; Kapteijn, F. Sulfation of Metal-Organic

Frameworks: Opportunities for Acid Catalysis and Proton Conductivity. *J. Catal.* **2011**, *281*, 177–187.
(65) Miao, Z.; Qi, C.; Wensley, A. M.; Luan, Y. Development of a Novel Brønsted Acid UiO-66 Metal-Organic Framework Catalyst by Postsynthetic Modification and Its Application in Catalysis. *RSC Adv.* **2016**, *6*, 67226–67231.
(66) Miao, Z.; Zhou, Z.; Tang, H.; Yu, M.; Ramella, D.; Du, X.; Luan, Y. Homodimerization of 2: H -Chromenes Catalyzed by Brønsted-Acid Derived UiO-66 MOFs. *Catal. Sci. Technol.* **2018**, *8* DOI: 10.1039/x0xx00000x.
(67) Kerber, S. J.; Bruckner, J. J.; Wozniak, K.; Seal, S.; Hardcastle, S.; Barr, T. L. The Nature of Hydrogen in X-Ray Photoelectron Spectroscopy: General Patterns from Hydroxides to Hydrogen Bonding. *J. Vac. Sci. Technol. A* **1996**, *14*, 1314-1320.

Table of Contents artwork: